Filtered density functions from direct numerical simulation of a reactive jet in cross-flow

R. W. Grout[a], E. S. Richardson[a], A. Gruber[b], C. S. Yoo[c], J. H. Chen[a]

[a] *Combustion Research Facility, Livermore, California.*
[b] *SINTEF Energy Research, Trondheim, Norway.*
[c] *Ulsan National Institute of Science and Technology, Ulsan, South Korea.*

Abstract

Direct numerical simulation (DNS) with multi-step hydrogen-air chemical kinetics is used to investigate the near-field of a flame stabilized above a reactive jet in cross-flow (JICF). JICF configurations are typically used where rapid mixing is desirable; classical applications are fuel injection nozzles and dilution holes in gas turbine combustors. Due to the computational cost of DNS, approximate solution methods such as large-eddy simulation (LES) are essential to parametrically study the effect of changing fuel jet configurations on the far field, but these methods require submodels capable of accurately capturing the near-field flame stabilization for success. By incorporating a wealth of turbulence-chemistry interactions (between the flame and vorticity generated by the jet shear layer instability as well as product recirculation by a large counter-rotating vortex pair), this DNS is exceptionally well suited to exploration of unclosed terms in LES formulations such as the chemical source-term. One quantity of direct relevance to several models for stratified combustion, such as the Bray-Moss (BM) model and doubly-conditional source-term estimation (DCSE), is the filtered density function for the mixture fraction ξ and partially premixed progress variable c. Empirical extraction of the filtered density functions of progress variable and mixture fraction at two representative locations demonstrates the complexity of approximating these two functions from a one- or two-parameter functional form.

Keywords:
Direct numerical simulation, transverse jet, hydrogen, partially premixed combustion, subgrid model

1. Introduction

Global reduction of greenhouse-gases and pollutant emissions has become an important issue for the energy sector and in this respect hydrogen-rich gases have emerged as candidate fuels in pre-combustion CO_2 separation scenarios, for large scale power generation with carbon capture and storage (CCS), and in the context of coal gasification (IGCC). While gas turbine combustors burning hydrocarbon fuels in lean premixed (LPM) mode have reached a high level of maturity [1], only moderate success has been achieved by gas turbine manufacturers in developing efficient, environmental friendly, combustion chambers that burn hydrogen-rich fuels and operate safely and reliably in LPM mode [2]. One of the first and most serious design challenges for the premixer section of such hydrogen-fired combustors is the issue of fuel injection. High reactivity of the hydrogen fuel when injected into the relatively hot oxidant stream exiting the compression stage complicates identifying a fuel injection configuration that does not allow flame stabilization in the near field of the fuel injection nozzle. This is critically important, as it ensures intrinsic (passive) flashback safety of the fuel injection system: in the eventuality that an off-design transient event allows the flame to propagate upstream of its design position inside the premixer, an intrinsically safe fuel injection system is able to flush the flame out of the premixer as soon as the off-design transient has receded. A design providing anchoring locations is therefore unacceptable, so a clear understanding of the mechanism for flame anchoring in this configuration is a valuable design aid.

The objective of the present work is to shed light on the unresolved features when a fully resolved solution for such a jet is subjected to filtering operations. In Reynolds-Averaged Navier Stokes (RANS) or Large Eddy (LES) simulations, such unresolved behavior must be accounted for. Modelling partially premixed combustion requires non-trivial extensions beyond pre-

mixed flame models. Utilizing a presumed form for the subgrid distribution of markers for mixture preparation (mixture fraction) and flame propagation (progress variable) requires that the presumed form for the subgrid pdfs be capable of effectively representing the distribution.

JICF configurations are characterized by a high degree of unsteadiness and by large-scale coherent vortical structures that form in the wake of the transverse jet [3]. These structures stretch the interface and increase the area available for molecular mixing which increases the mixing rate, facilitating combustion. Previous DNS studies of inert JICF configurations [4, 5, 6, 7, 8] have shown that several factors, e.g.: the momentum ratio between the transverse jet and the cross flow, the shape of the nozzle, the angle of injection, the thickness of the approaching cross-flow boundary layer, influence the flow and scalar mixing fields. Further, Hasselbrink and Mungal [9] showed observed experimentally that heat release in a reacting case can influence the overall rate of cross flow fluid entrainment.

Direct numerical simulation (DNS) of the reactive JICF studied here provides detailed information about the flow structures and turbulence-chemistry interaction which facilitate flame stabilization. In addition to fully resolving the turbulent velocity fields, the two-way coupling between the heat release and the flow field is accurately accounted for using multi-step chemical kinetics [10] and molecular transport mechanism. DNS is uniquely capable of providing the necessary information about the turbulent flow and on its interaction, at a microscale level, with combustion chemical kinetics to facilitate model testing and development. The numerical simulation presented here, characterized by a square jet nozzle geometry, is the first part of a parametric study of inert and reactive JICF configurations that includes several other nozzle shapes, injection angles, momentum ratios and turbulence levels.

The remainder of this paper is organized as follows: Section 2 gives an overview of the numerical method and case configuration, then Section 3 presents the key results. Finally, Section 4 summarizes the main findings and provides an outline of future planned work.

2. Mathematical Description And Configuration

The Navier-Stokes equations in their compressible formulation are solved on a 3-D computational domain using the finite-difference solver S3D [11]. The boundary conditions are configured to simulate a turbulent flame stabilized in the wake of a transverse laminar fuel jet exiting a blunt squared nozzle[1] orthogonally into a turbulent boundary layer cross flow over a flat plate. The wall is assumed inert and no surface reactions are considered while gas-phase low-temperature recombination reactions of radical species at the wall are taken into account. The mechanism from [10] is used to represent hydrogen-air chemical kinetics including 9 species and 19 reactions.

Figure 1 depicts an instantaneous illustration of the solution and includes volume renderings of the hydrogen, temperature and HO_2 radical scalar fields.

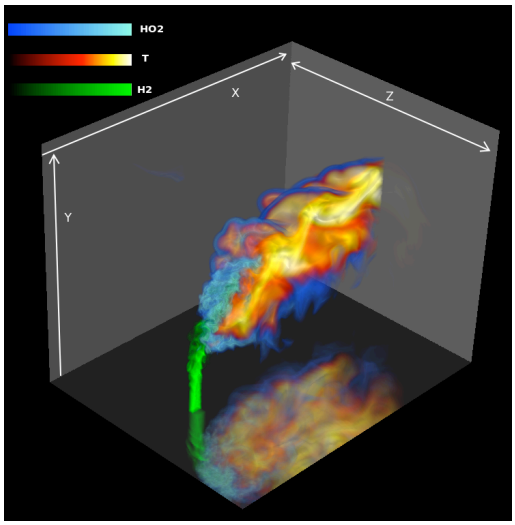

Figure 1: Volume rendering of temperature (black body colormap), HO_2 (blue colormap), and H_2 (green colormap) scalar fields at t=2.802ms from start of simulation. Opacity transfer functions adjusted to highlight the regions with high temperature, HO_2, or H_2 mass fraction.

The turbulent cross flow enters the computational domain from a non-reflecting inflow boundary. As the cross flow direction is not homogeneous in the presence of the transverse jet and of the flame, the recycling procedure described in [12] cannot be used. Therefore, an auxiliary DNS of an inert turbulent flow over a flat plate is used to provide the reactive case with the initial turbulent field and inlet turbulence. The auxiliary simulation is performed at lower resolution ($\Delta \sim 100\mu m$); the auxiliary grid is comprised of $384 \times 240 \times 300$ points spanning physical dimensions 40mm $\times$ 20mm $\times$ 20mm in the x,y,z directions. Periodic boundary conditions are applied in the spanwise and streamwise directions and the flow is driven by a body force acting in the stream-

[1] The choice of the squared nozzle shape for the first part of the ongoing parametric study is motivated by its simplicity in the context of the Cartesian grids used in DNS.

wise direction. The viscous length scale is measured *a posteriori* as $\delta_\nu = 35.4\,\mu m$ and the friction velocity $u_\tau = 2.1 m/s$. Since the domain length is $> 1000\delta_\nu$, we expect it to be sufficiently large to adequately capture the boundary layer structures necessary for realistic feed data. After 4 flow through times based on the mean cross flow velocity ($u_{\mathrm{cf}} = 55 m/s$) a realistic boundary layer is established and sampled over continued evolution. Although the turbulent feed data is time evolving, the increase in the boundary layer thickness is very small between the start and end times of the main flame simulation. The boundary conditions are implemented following the method described in [13] and [14], including the successful improvements of [15] and [16]. For the main simulation, the boundary conditions are: non-reflecting at the inflow ($x = 0$) and outflow ($x = L_x$,$y = L_y$) planes, no-slip isothermal solid surface at the wall boundary ($y = 0$), and periodic in the spanwise direction ($z = 0$ and $z = L_z$). The temperature of the wall and of the cross flow air is set to 750 K while the fuel jet temperature is set to 420 K.

2.1. Reacting DNS

The three-dimensional Cartesian grid used for the production simulation is uniform in the stream-wise and span-wise directions and is refined in the wall-normal direction near the solid surface using a *tanh* mapping. The production grid is comprised of $1.6 \cdot 10^9$ points arranged as $1408 \times 1080 \times 1100$ in the x,y,z directions with physical domain dimensions 25mm × 20mm × 20mm. The first point off the wall is at $y^+ = 0.33$ where the superscript + indicates non-dimensionalization by the viscous length scale δ_ν computed from the feed data. The production grid resolution is $\Delta x^+ \sim 0.5$ ($\Delta x = 17.8$ μm), $\Delta y^+ \sim 0.3$–0.7 ($\Delta y = 10.2$–$24.3\,\mu$m) and $\Delta z^+ \sim 0.5$ ($\Delta z = 18.2\mu$m). The simulation is run on 48 000 cores of *Jaguar*, the Cray XT5 at ORNL, and used approximately 4M cpu hours.

$\mathrm{Re_{jet}}$	$\mathrm{T_{jet}}$	$\mathrm{T_{cf}}$	u_j/u_{cf}	$\sqrt{\rho_j u_j^2/\rho_{cf} u_{\mathrm{cf}}^2}$	$u'_{\mathrm{cf}}/u_{\mathrm{cf}}$
3980	423k	750k	4.5	3.4	0.1

Table 1: Simulation parameters ($\mathrm{Re_{jet}}$ is based on hydraulic diameter)

The velocity field for the production simulation is initialized with the velocity field present in the auxiliary domain at the instant the feed data sampling was started. After transitioning the jet inlet velocity to its final value over $10\mu s$, the simulation is advanced an additional flow-through time to establish the fuel plume. Next, reaction is enabled and a 'flame anchor', consisting of a notional heated rod, is placed in the flow to coincide with flammable mixture for only 8 μs before it is removed. Once all of the fluid present in the domain when the flame anchor is removed exits through the outflow boundary, the solution is up-sampled to the production grid.

3. Results and Discussion

The DNS results can be post-processed by temporal averaging or spatial filtering as appropriate to consider the solution in either the RANS or LES paradigm. In this section we will consider the temporally averaged avenue only so far as to indicate how the instantaneous fields relate to the statistically stationary behavior.

To parametrize the flame front two variables are used: a mixture fraction ξ computed using the hydrogen and oxygen elemental mass fractions and a progress variable c defined with reference to the local mixture fraction. Such a progress variable is a useful flame marker which is frequently used for stratified premixed flames, e.g. [21]:

$$c \equiv \frac{Y_{H_2O} - Y_{H_2O,u}(\xi)}{Y_{H_2O,b}(\xi) - Y_{H_2O,u}(\xi)}, \tag{1}$$

where the burnt and unburnt states are defined with respect to an appropriate reference configuration. Here, we chose complete combustion for the burnt reference state.

3.1. Mean flame stabilization

Time averages of the mean quantities were accumulated over a 0.4ms window using 50 snapshots of the solution saved at $8\mu s$ intervals. The resulting time averaged solution on the midplane in the spanwise direction is shown in the top (mixture fraction, normalized heat release rate) and bottom (normalized heat release rate, velocity magnitude) parts of Figure 2. From the heat release contours, we can see that the flame stabilizes, on average, at 1.5–2 jet widths downstream and 3–5 jet heights from the jet exit. The peak heat release is coincident with a region where the magnitude of the average flow velocity is locally low and the average mixture fraction $\overline{\zeta} = 0.171$ is near stoichiometric (the stoichiometric mixture fraction is $\zeta_{\mathrm{st}} = 0.169$). The isolines in Figure 3 show where the magnitude of the mean velocity falls below 25m/s, or approximately 10% of the maximum velocity in the domain; the vectors indicate the in-plane velocity. In the spanwise direction, the peak heat release is located on the center-line, just above and between the large counter-rotating vortex pair which has been identified in non-reactive jet-in-cross-flow studies

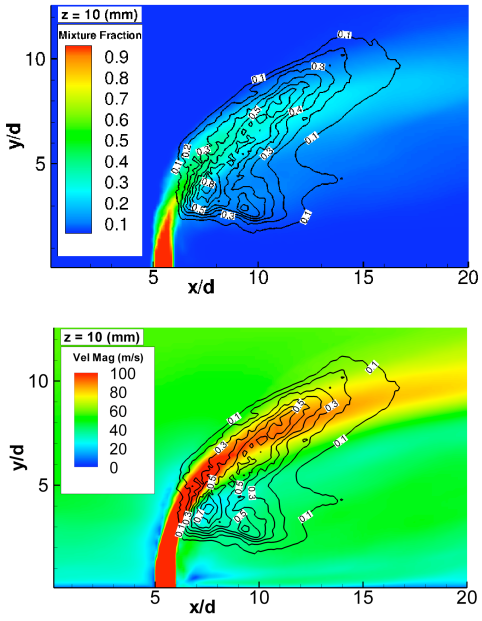

Figure 2: Slices on the midplane showing RANS averaged solution for mixture fraction and normalized heat release rate (top) and velocity magnitude and normalized heat release rate (bottom).

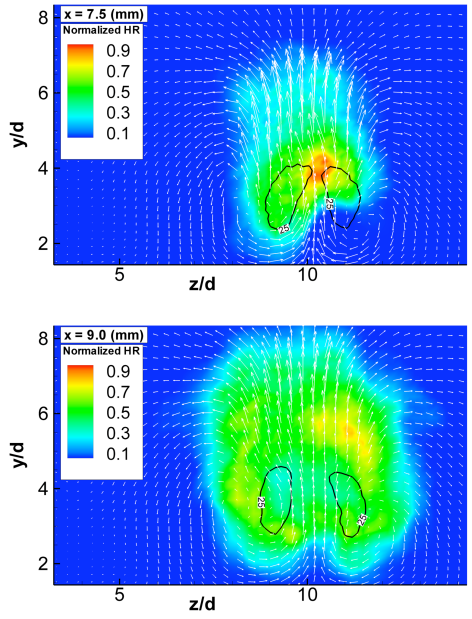

Figure 3: Slices orthogonal to mean flow direction showing RANS averaged solution for heat release rate normalized by peak heat release rate, in-plane velocity vectors, and isolines for the mean velocity magnitude.

[3] as contributing significantly to mixing between the jet and cross-flow fluids [8].

3.2. *Instantaneous solution*

The instantaneous solution is shown on the midplane in Figure 4 where the mixture fraction is overlayed with contours of instantaneous heat release. Comparison of this figure with Figure 5, where the corresponding spatially filtered solution is shown, illustrates the loss of fidelity from the filtering operation. The spatial filtering was performed using a top-hat filter of width 0.5mm (one-half of the characteristic jet dimension).

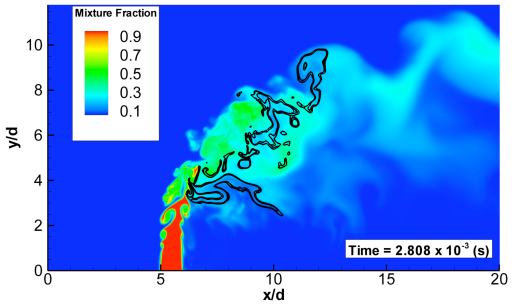

Figure 4: Slice on the midplane showing instantaneous mixture fraction at t=2.808ms. Lines represent $8 \cdot 10^9$ and $1 \cdot 10^{10} J/m^3/s$ isocontours of the instantaneous heat release rate.

In Figure 5, we can identify two qualitatively differing portions of the flame front. In the vicinity of $y/d \sim 5$–10, $x/d \sim 7$–12 is a region where the flame is thickened in Figure 5 and the situation is highly visibly intermittent with respect to both composition and heat release in Figure 4. This region corresponds to the location where the majority of the heat release occurs in the temporal mean (see Figure 2). Downstream of this region, the flame front is less intermittent, the instantaneous and mean heat release is lower, and the flame front is visibly more compact.

In Figure 6, empirical subgrid pdfs computed by normalizing histograms extracted from the DNS are shown for the intermittent, high heat release region. The pdfs show how the subgrid distribution of the partially premixed progress variable (Equation 1) and mixture fraction varies through the primary heat release zone. The series in the plots in Figure 6 are all taken from the midplane at $y/D = 5$; the individual series span $x/D = 7.5$ through $x/D = 10$. Through the filtered flame front, the pdf develops a peak between $c \sim 0.1$–0.2 and the unburnt gas fraction drops. Near the center of the reaction zone the subgrid pdf is almost entirely comprised of partially burnt gas ($x/D \sim 8.75$). Near the back side of the flame, a peak develops around $c \sim 0.8$ which then evolves towards the fully burnt state. At the same time, the mixture fraction pdf is very broad, indicative of the intermittency in composition at this location,

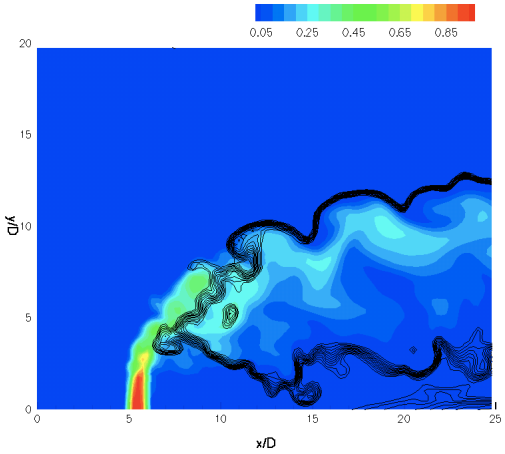

Figure 5: Slice on the midplane showing filtered mixture fraction at t=2.808ms. Lines represent isocontours of the instantaneous progress variable from $c = 0.2$ through $c = 0.8$.

and evolves significantly across the flame front. This rapid evolution suggests that the mixing and reaction timescales are comparable.

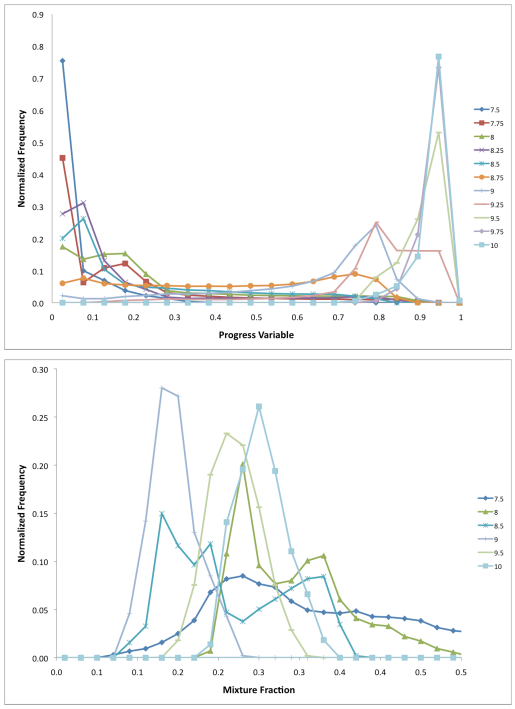

Figure 6: Variation of normalized histogram of progress variable and mixture fraction along $y/D = 5$ from $x/D = 7.5$–10. Histogram is normalized to form empirical pdfs $p(c)$ and $p(\xi)$

In Figure 7, similarly obtained pdfs are shown on the midplane at $x/D = 14$, $y/D = 8.5$–10.75, where the heat release is lower and the flame front resembles a conventional laminar flamelet. At this location the fuel and oxidizer are more fully mixed and the distribution of mixture fraction far narrower than at the previous location shown in Figure 6. Across the flame front a similar trend is apparent in the progress variable distribution: partially burnt gas with progress variable $c \sim 0.8$ is present in significant quantity in many of the filter volumes across the flame front. The persistent peak in the pdf at $c < 1.0$ suggests that approximating this empirical pdf with a conventional three part pdf (e.g., [22]) will be challenging.

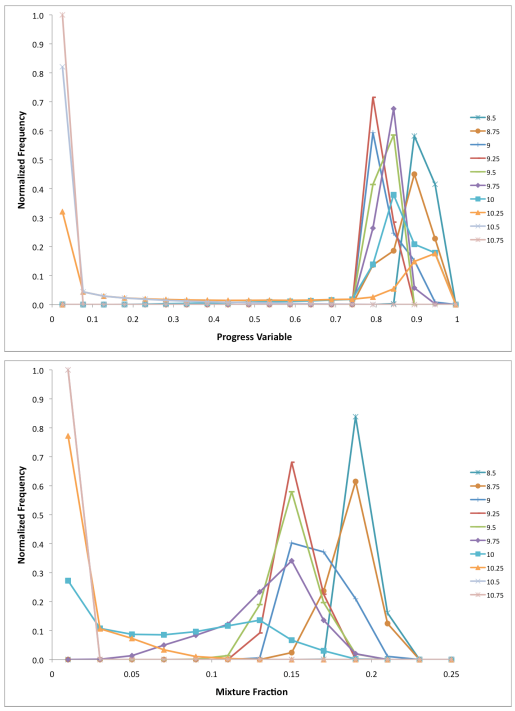

Figure 7: Variation of normalized histogram of progress variable and mixture fraction along $x/D = 14$, $y/D = 8.5$–10.75. Histogram is normalized to form empirical pdfs $p(c)$ and $p(\xi)$

4. Concluding Remarks

Approximation of the subgrid distributions of the mixture fraction and progress variable is a prerequisite for effective deployment of presumed pdf models in the LES context. In this work, we have shown that, for a filter width sufficiently small to partially resolve the flame front, the progress variable pdf has a challenging form. Promising approaches for approximating the pdf with a 3-part functional form, such as proposed by Bray et al. [22], may have difficulty reproducing the peak occurring at $c < 1$. While this difficulty may be alleviated by

an alternate definition for the progress variable, doing so risks loosing the fidelity of the parametrization of the reaction zone. Future work is necessary to quantify the error in using presumed one- and two-parameter functional forms to approximate such pdfs, and to determine the degree to which the joint pdf of progress variable and mixture fraction may be separable.

Acknowledgements

Computational support for this project was supported by and this research used resources of the National Center for Computational Sciences at Oak Ridge National Laboratory, which is supported by the office of Science of the US Department of Energy under contract DE-AC05-00OR22725. The work at Sandia National Laboratories was supported by the Division of Chemical Sciences, Geosciences, and Biosciences, Office of Basic Energy Sciences of the US Department of Energy and by the US Department of Energy SciDAC Program. SNL is a multiprogramme laboratory operated by Sandia Corporation, a Lockheed Martin Company for the US DOE under Contract DE-AC04-94AL85000. The authors would like to acknowledge the help of Dr. Hongfeng Yu in preparing the volume rendering in Figure 1. The work at SINTEF is supported by the Climit Program of the Research Council of Norway and Gassnova.

References

[1] K. Döbbeling, J. Hellat and H. Koch, "25 Years of BBC/ABB/Alstom Lean Premix Combustion Technologies", *ASME Journal of Engineering for Gas Turbines and Power*, 129 (2007) 2–12.

[2] P. Chiesa, G. Lozza, and L. Mazzocchi, "Using Hydrogen as Gas Turbine Fuel", *ASME Journal of Engineering for Gas Turbines and Power*, 127 (2005) 73–80.

[3] T.F. Fric and A. Roshko, "Vortical Structure in the Wake of a Transverse Jet", *Journal of Fluid Mechanics*, 279 (1994) 1–47.

[4] S. Muppidi and K. Mahesh, "Study of Trajectories of Jets in Crossflow Using Direct Numerical Simulations", *Journal of Fluid Mechanics*, 530 (2005) 81–100.

[5] S. Muppidi and K. Mahesh, "Two-Dimensional Model Problem to Explain Counter-Rotating Vortex Pair Formation in a Transverse Jet", *Physics of Fluids*, 18 (2006) 085103-1–9.

[6] S. Muppidi and K. Mahesh, "Direct Numerical Simulation of Round Turbulent Jets in Crossflow", *Journal of Fluid Mechanics*, 574 (2007) 59–84.

[7] S. Muppidi and K. Mahesh, "Direct Numerical Simulation of Passive Scalar Transport in Transverse Jets", *Journal of Fluid Mechanics* 598 (2008) 335–360.

[8] M. Salewski, D. Stankovic and L. Fuchs, "Mixing in Circular and Non-circular Jets in Crossflow", *Flow, Turbulence and Combustion*, 80 (2008) 255–283.

[9] E.H. Hasselbrink and M.G. Mungal, "Transverse jets and jet flames. Part 2. Velocity and OH field imaging", *Journal of Fluid Mechanics*, 443 (2001) 27–68.

[10] J. Li, Z. Zhao, A. Kazarov and F.L. Dryer, "An Updated Comprehensive Kinetic Model of Hydrogen Combustion", *International Journal of Chemical Kinetics*, 36 (2004) 566–575.

[11] J.H. Chen, A. Choudhary, B. de Supinski, M. DeVries, E.R. Hawkes, S. Klasky, W.K. Liao, K.L. Ma, J. Mellor-Crummey, N. Podhorski, R. Sankaran, S. Shende and C.S. Yoo, "Terascale direct numerical simulations of turbulent combustion using S3D", *Computational Science and Discovery*, 1 (2008).

[12] P.R. Spalart, M. Strelets and A. Travin, "Direct Numerical Simulation of Large-Eddy-Break-Up Devices in a Boundary Layer", *International Journal of Heat and Fluid Flow*, 27 (2006) 902–910.

[13] K. W. Thompson, *Journal of Computational Physics*, 68 (1987) 1–24.

[14] K. W. Thompson, *Journal of Computational Physics*, 89 (2) (1990) 439–461.

[15] T. Poinsot and S. K. Lele, *Journal Computational Physics*, 101 (1) (1992) 104–139.

[16] J. C. Sutherland, and C. A. Kennedy, *Journal of Computational Physics*, 191 (2003) 502–524.

[17] H. Yamashita, M. Shimada and T. Takeno, "A numerical study on flame stability at the transition point of jet diffusion flames", *Proceedings of the Combustion Institute* 26 (1996) 24–34.

[18] M.S. Chong, A.E. Perry, and B.J. Cantwell, "A general classification of three-dimensional flow fields", *Phys. Fluids A* 2(5) (1990) 765–777,

[19] M. Tanahashi, M. Fujimura and T. Miyauchi, "Coherent fine-scale eddies in turbulent premixed flames", *Proceedings of the Combustion Institute* 28 (2000) 529–535.

[20] N. Peters *Turbulent Combustion* Cambridge University Press (2000).

[21] K. Bray, P. Domingo and L. Vervisch, "Role of the progress variable in models for partially premixed turbulent combustion", *Combustion and Flame*, 141 (2005) 431–437.

[22] K.N.C. Brary, M. Champion, P. Libby, and N. Swaminathan, "Finite rate chemistry and presumed PDF models for premixed turbulent combustion", *Combustion and flame*, 14 (2006) 665.